A Phantom Study for Attenuation Change and Detection of Calcification in Lung Nodules According to Variation of Examination Techniques in Low Dose CT

by

Jae Yong Cho

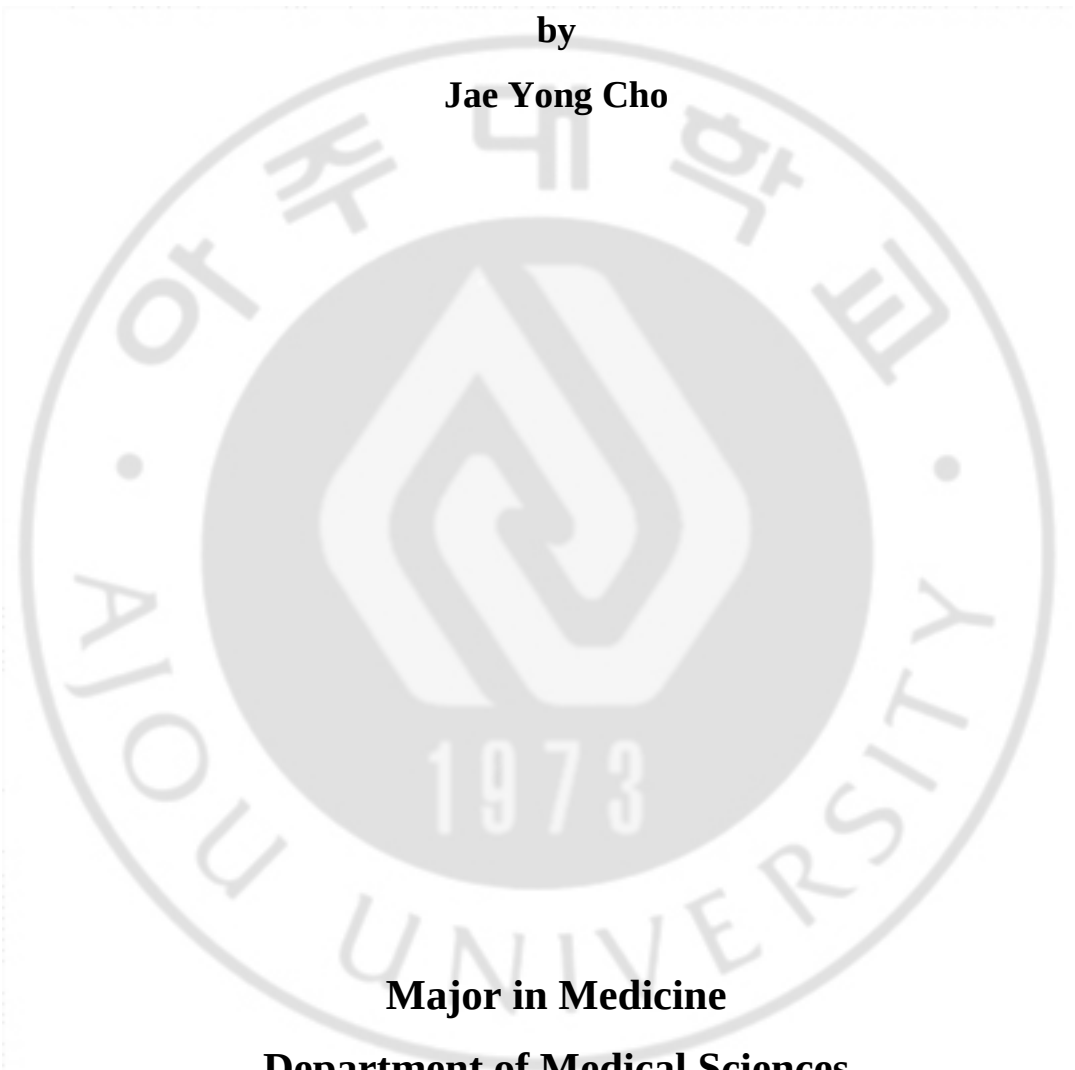

Major in Medicine

Department of Medical Sciences

The Graduate School, Ajou University

A Phantom Study for Attenuation Change and Detection of Calcification in Lung Nodules According to Variation of Examination Techniques in Low Dose CT

by

Jae Yong Cho

A Dissertation Submitted to The Graduate School of
Ajou University in Partial Fulfillment of the Requirements for the Degree of Master of Medicine

Supervised by
Kyung Joo Park, M.D., Ph.D.

Major in Medicine
Department of Medical Sciences
The Graduate School, Ajou University

This certifies that the dissertation

of Jae Yong Cho is approved.

SUPERVISORY COMMITTEE

Kyung Joo Park

Joo Sung Sun

Joo Hun Park

The Graduate School, Ajou University

December, 18th, 2015

ABSTRACT

Purpose : To evaluate the attenuation change of hyperdense lung nodule and diagnostic performance of visual assessment according to various tube voltage and current setting in low-dose CT comparing with standard-dose CT.

Material and Methods : A chest phantom containing artificial nodules was scanned with 64-detector-row and 128-detector-row CT scanners using a standard and various low-dose settings with iterative reconstruction. Mean attenuation of nodules and image noise were compared between the standard-dose and low-dose images. Diagnostic accuracy of visual assessment by two readers for discrimination of hyperdense nodule was analyzed using CT images of standard and 5 selected low-dose settings.

Results : Mean CT attenuation of nodules was increased with low tube voltage and image noise was increased with low tube voltage and current in both CT scanners. Mean attenuation of some nodules below hyperdense criteria (200 HU) on standard-dose CT was changed to considerably above 200 HU on low tube current and voltage setting. Diagnostic accuracy for discrimination of hyperdense nodule by visual

assessment was not different between standard-dose and low-dose CT scans. Inter-observer agreement for grading of hyperdense nodule showed better agreement in higher radiation-dose scans.

Conclusion : Low-dose CT maintains the diagnostic accuracy in visual assessment of hyperdense lung nodule despite increased image noise and higher attenuation criteria will be necessary for determining hyperdense nodule using CT densitometry in low-dose setting.

Keywords : Low-dose chest CT, Lung phantom, Lung nodule, CT densitometry

TABLE OF CONTENTS

ORDER OF FIGURES

ORDER OF TABLES

I. INTRODUCTION

Recently, low-dose chest CT examinations are widely used for screening of lung cancer due to the results of studies that proved a reduced lung cancer related mortality in a high risk group using low-dose CT as a screening method[1-4]. However, low-dose CT imaging has a limitation of poor image quality which can reduce the diagnostic accuracy. Some authors proposed the appropriate tube currents and tube voltages of screening low-dose CT without loss of diagnostic quality, but it remains on the debate[5-10]. For improving image quality, iterative reconstruction technique was introduced. Many reports showed that iterative reconstruction algorithm reduces image noise and improves both objective and subjective image quality, compared with filtered back projection (FBP) on chest CT even though the same dose of radiation is delivered[5, 11-15].

A mean CT attenuation of lung nodule was advocated as a good discriminator of benignity[16-18]. Previous reports showed that high mean CT attenuation of lung nodule can be considered as a favorable sign of benignity[16,18]. It was presumed that diffuse calcification likely accounts for the higher CT numbers of some benign

lesions[17]. Proto et al. suggested that hyperdense nodules with a CT attenuation above 200 HU were benign, while evident calcification was not shown on conventional radiograph[16]. Siegelman et al. suggested representative CT attenuation above 164 HU in lung nodule could be deemed benign[18]. However, these results cannot be directly applied to low-dose CT scan, because the CT attenuation changes according to the alteration of tube parameters. To the best of our knowledge, there has been no previous study about an effects of examination techniques of low-dose CT using iterative reconstruction on the attenuation change of lung nodules and detection of calcification.

The purpose of this phantom study was to evaluate the attenuation change of lung nodule and the diagnostic performance of visual assessment according to various setting of examination techniques in low-dose CT using iterative reconstruction.

II. MATERIAL AND METHODS

A. Anthropomorphic Phantom and Artificial Nodules

A commercially available lung phantom (Chest phantom N1 Lungman, Kyoto Kagaku Co., Ltd, Kyoto, Japan) was used. Fourteen artificial phantom nodules were created by mixtures of polyvinyl alcohol, calcium carbonate, and 3% solution of borax. Spherical shaped nodules were in two different sizes (7 mm and 10 mm). Each nodule had a variable concentration of calcium carbonate so that mean CT attenuations of 14 nodules ranged from 80 to 410 HU when measured on CT images obtained with standard dose (120 kVp / 100 mAs) (Table 1-4). The artificial nodules were made to have round to oval shapes and smooth or slightly irregular surface. Internal attenuation of nodules had a variety of heterogeneity with the range of standard deviation from 21 to 118 HU on CT images obtained with standard dose. These nodules were placed randomly between vascular structures of the lung phantom similar to parenchymal lung nodules without direct contact with the mediastinum and chest wall. (Fig. 1 and 2)

Table 1. CT attenuation of the phantom nodules in 128-detector-row CT scan

		Nodule Size = 10 mm						
		Nodule 1	Nodule 2	Nodule 3	Nodule 4	Nodule 5	Nodule 6	Nodule 7
Tube Parameter (kVp/mAs)	DLP (mGycm)	CT Attenuation (HU, Mean ± SD)						
120/100	230	82.4±32.6	144.4±26.0	171.5±27.0	202.8±27.0	250.5±60.0	282.9±75.8	316.3±94.3
120/40	92	80.3±35.8	143.4±35.4	162.8±44.2	209.6±30.9	246.4±61.1	267.2±80.1	319.9±100.0
120/20	47	72.2±51.5	144.4±47.3	178.6±44.4	196.7±40.5	239.4±66.3	272.4±72.4	334.0±115.2
120/15	34	75.0±48.4	154.2±44.2	164.5±34.1	191.8±61.1	251.0±71.6	274.7±81.1	309.6±110.3
120/10	23	61.1±58.5	145.2±53.7	162.3±53.7	194.0±53.0	258.9±52.2	267.8±92.9	334.4±112.5
100/100	140	60.0±47.1	141.9±31.2	176.0±26.7	205.7±31.4	262.4±69.8	299.0±84.9	356.8±111.7
100/.40	56	68.9±46.0	144.2±41.3	170.1±31.9	215.6±38.0	272.2±73.3	296.3±85.7	357.6±114.9
100/20	29	73.4±61.2	145.6±43.4	170.3±49.3	208.4±49.7	282.3±70.9	305.4±89.9	338.6±128.5
100/15	21	56.1±90.0	151.2±54.9	178.7±46.5	210.8±72.3	274.5±71.3	312.2±107.2	350.4±123.1
100/10	14	53.4±78.4	158.3±73.3	164.5±70.7	213.1±60.1	271.8±75.0	314.7±105.9	359.0±148.3
80/100	66	56.4±54.0	140.7±45.7	171.3±35.7	216.8±45.9	307.4±80.5	346.6±110.8	387.8±125.9
80/40	27	67.7±60.1	144.4±48.9	168.1±54.8	216.6±62.0	303.3±90.7	349.4±116.5	394.8±132.4
80/20	14	63.5±98.9	135.4±77.5	187.4±70.6	238.0±74.6	310.7±95.0	362.5±123.7	395.0±171.7
80/15	10	63.2±111.0	147.2±84.1	159.8±69.5	226.3±74.4	292.9±104.3	365.9±138.2	420.8±179.4
80/10	7	76.8±196.5	134.1±103.1	192.9±70.1	228.8±109.3	280.3±132.7	361.8±180.1	398.4±198.1

Table 2. CT attenuation of the phantom nodules in 128-detector-row CT scan

		Nodule Size = 7 mm						
		Nodule 8	Nodule 9	Nodule 10	Nodule 11	Nodule 12	Nodule 13	Nodule 14
Tube Parameter (kVp/mAs)	DLP (mGy*cm)	CT Attenuation (HU, Mean ± SD)						
120/100	230	98.8±21.2	148.5±26.5	169.2±22.6	216.8±33.7	251.4±65.9	270.9±118.0	308.1±52.2
120/40	92	93.7±40.8	153.7±35.1	178.6±33.7	210.2±32.3	246.8±69.4	273.8±105.5	314.7±45.1
120/20	47	99.0±52.4	158.0±57.8	177.2±47.2	204.7±55.0	256.6±83.5	277.1±116.1	329.5±63.1
120/15	34	105.3±47.6	157.8±44.6	167.6±52.3	216.5±55.0	240.9±63.5	280.9±112.8	324.7±45.6
120/10	23	85.8±65.2	142.1±48.9	171.0±55.8	225.1±64.5	250.5±65.7	286.9±121.2	321.8±39.0
100/100	140	86.2±18.9	156.9±28.1	175.8±26.1	215.2±44.5	281.6±77.1	287.5±123.4	351.5±79.8
100/.40	56	95.8±34.8	151.6±51.4	177.7±30.0	228.8±54.6	271.5±63.9	298.8±121.8	344.1±52.6
100/20	29	96.1±64.0	151.0±46.2	175.2±46.3	226.6±84.9	278.8±66.9	299.1±144.2	338.8±51.5
100/15	21	110.1±78.6	144.9±46.1	176.1±56.9	251.7±95.8	275.7±98.3	300.4±135.0	351.8±88.6
100/10	14	102.2±71.8	179.1±90.6	175.0±83.1	228.6±99.0	292.1±118.7	352.6±172.8	329.5±98.6
80/100	66	89.1±53.2	165.9±34.5	171.5±36.2	241.3±42.2	313.9±92.2	355.9±158.4	406.0±64.0
80/40	27	97.0±55.6	159.6±77.0	167.4±50.0	248.8±52.1	312.9±93.3	357.8±178.9	393.9±87.5
80/20	14	72.2±113.4	174.0±101.4	178.7±86.4	245.1±97.8	316.7±77.3	373.0±201.2	401.6±96.2
80/15	10	84.7±124.1	185.7±85.1	177.9±106.3	261.1±120.7	329.2±121.1	374.9±239.6	405.1±99.6
80/10	7	84.0±119.4	203.1±163.6	200.0±89.4	223.5±115.9	318.4±151.1	355.1±196.7	419.1±115.9

Table 3. CT attenuation of the phantom nodules in 64-detector-row CT scan

		Nodule Size = 10 mm						
		Nodule 1	Nodule 2	Nodule 3	Nodule 4	Nodule 5	Nodule 6	Nodule 7
Tube Parameter (kVp/mAs)	DLP (mGy*cm)	CT Attenuation (HU, Mean ± SD)						
120/100	229	109.4±35.8	174.5±26.9	203.3±24.1	233.6±26.0	307.7±56.9	320.8±72.3	402.7±64.9
120/40	91	111.9±54.9	183.3±42.3	202.5±38.7	232.9±41.6	300.3±51.6	318.5±79.0	404.8±69.5
120/20	46	113.5±61.8	174.1±36.9	203.6±40.0	232.2±45.3	306.2±61.1	318.0±74.7	401.8±97.6
120/15	34	116.5±77.8	184.7±50.2	196.3±55.4	229.7±63.6	300.1±52.9	309.8±61.0	396.1±89.9
100/100	138	101.6±43.1	179.6±23.5	193.3±31.8	239.0±48.5	322.0±53.9	345.6±85.1	437.6±78.5
100/.40	55	103.4±51.6	174.0±38.8	203.9±43.0	239.9±34.4	327.9±61.6	342.4±95.9	432.0±94.0
100/20	28	103.9±74.3	183.8±52.4	203.0±63.5	242.8±74.0	315.6±76.2	354.9±77.9	437.0±125.3
100/15	21	95.1±78.3	179.4±70.1	191.1±68.3	243.6±76.5	321.0±73.8	346.3±92.7	450.2±106.7
80/100	66	100.9±52.5	181.2±45.8	209.5±47.1	255.7±48.1	364.0±71.1	400.5±92.8	499.4±103.6
80/40	27	113.4±72.0	173.6±62.4	202.1±59.9	263.2±76.1	362.4±86.7	387.3±106.5	490.7±98.5
80/20	13	100.8±119.7	183.2±90.4	205.9±77.7	254.9±103.0	368.4±89.9	405.6±124.8	498.8±123.9
80/15	10	105.6±139.8	189.5±107.1	209.6±88.0	257.8±98.8	370.1±80.1	398.7±114.0	503.7±182.4

Table 4. CT attenuation of the phantom nodules in 64-detector-row CT scan

		Nodule Size = 7 mm						
		Nodule 8	Nodule 9	Nodule 10	Nodule 11	Nodule 12	Nodule 13	Nodule 14
Tube Parameter (kVp/mAs)	DLP (mGy*cm)	CT Attenuation (HU, Mean ± SD)						
120/100	229	123.0±38.2	183.2±32.3	199.2±29.2	248.9±24.1	288.3±30.8	303.6±95.8	349.9±53.7
10/40	91	130.3±41.5	185.0±48.1	204.3±40.4	250.4±36.2	283.9±42.7	314.0±99.4	359.4±49.6
120/20	46	136.2±84.1	188.6±57.5	203.8±56.3	250.9±49.4	286.6±50.8	317.6±95.9	344.7±62.2
120/15	34	142.1±72.5	196.2±65.0	181.7±67.0	249.3±52.4	280.3±55.9	313.0±105.2	356.8±54.4
100/100	138	118.3±55.2	202.1±34.8	205.8±28.0	255.2±30.0	298.6±62.3	326.9±109.4	388.3±58.8
100/.40	55	119.1±65.3	188.1±52.2	194.0±40.4	259.3±44.3	306.0±49.2	329.0±114.2	369.8±70.0
100/20	28	125.9±82.6	193.0±88.3	214.3±58.7	260.9±71.0	299.6±63.7	311.9±117.3	388.9±65.2
100/15	21	120.3±98.2	195.8±96.2	219.3±79.0	257.5±90.8	313.1±58.4	341.6±138.9	388.3±72.8
80/100	66	117.3±55.8	202.3±69.1	226.9±43.2	277.2±54.2	344.2±44.9	370.4±115.4	450.0±78.4
80/40	27	131.5±106.8	201.6±81.2	221.4±61.4	286.0±78.4	341.9±65.1	379.2±149.7	456.4±88.0
80/20	13	104.6±104.4	230.9±138.1	221.6±84.6	302.0±117.0	342.9±100.4	381.6±148.9	445.7±119.8
80/15	10	122.9±138.7	223.0±104.8	218.6±108.2	312.8±114.1	355.9±97.9	408.8±182.2	469.6±108.1

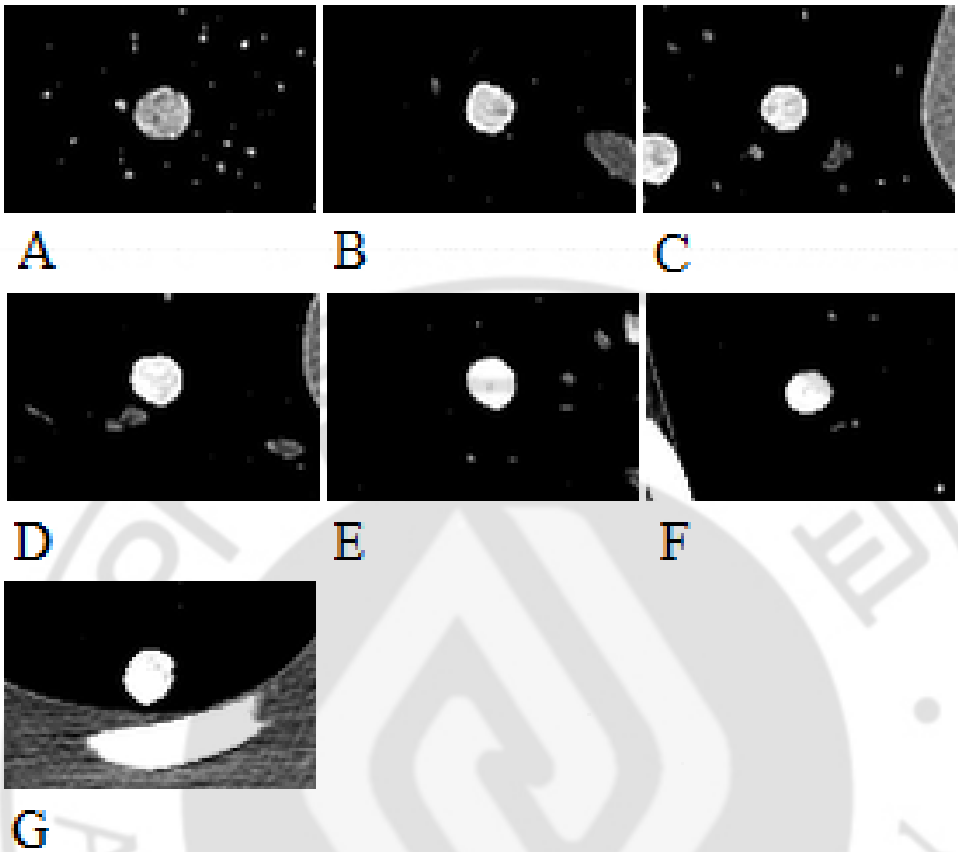

Figure 1. Standard dose CT images of 10-mm phantom nodules obtained with 128-detector row CT scanner. (Tube voltage/current = 120kVp/100mAs, Window width/level = 350/40)

(A) Nodule 1 (B) Nodule 2 (C) Nodule 3 (D) Nodule 4 (E) Nodule 5 (F) Nodule 6 (G) Nodule 7

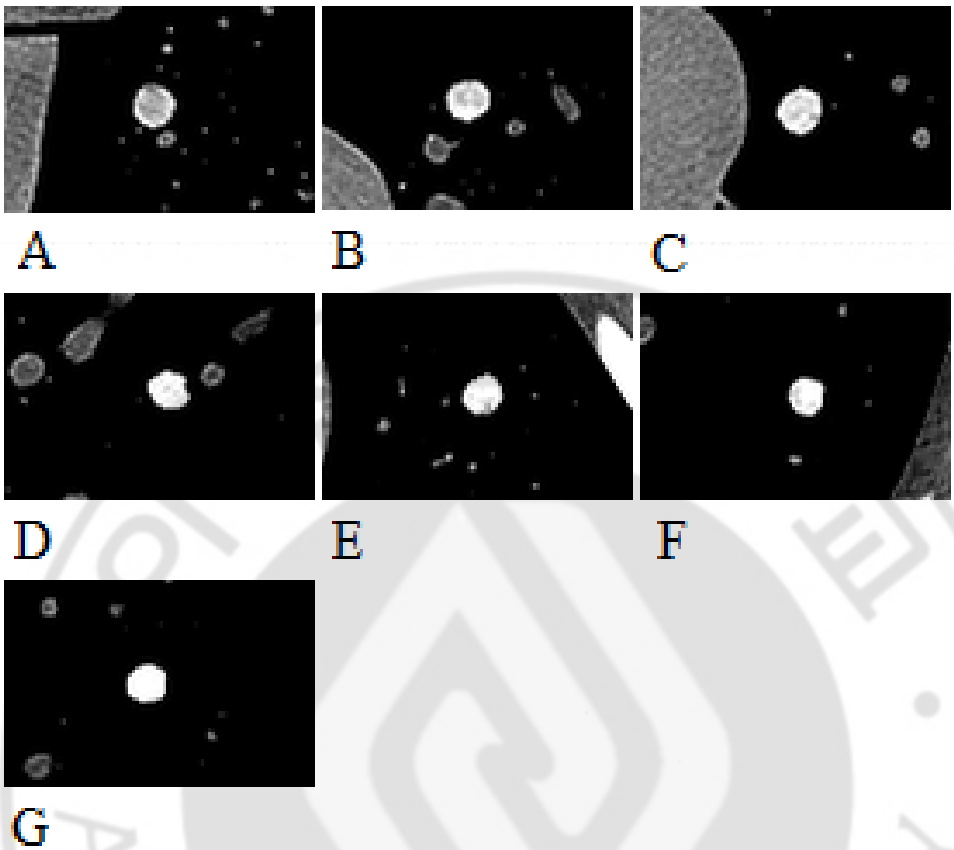

Figure 2. Standard dose CT images of 7-mm phantom nodules obtained with 128-detector-row CT scanner. (Tube voltage/current = 120kVp/100mAs, Window width/level = 350/40)

(A) Nodule 8 (B) Nodule 9 (C) Nodule 10 (D) Nodule 11 (E) Nodule 12 (F) Nodule 13 (G) Nodule 14

B. CT Imaging

CT images of the lung phantom containing artificial nodules were acquired using a 128-detector-row CT scanner (SOMATOM Definition, Siemens, Munich, Germany) and 64-detector-row CT scanner (Brilliance 64, Philips Healthcare, Andover, MA). Imaging was performed with a variable combinations of tube currents (15, 20, 40, 80, and 100 mAs in the both scanners and 10 mAs additionally in 128-dector-row scanner) and voltages (80, 100, 120 kVp), which resulted in eighteen and fifteen different protocols of each scanner. Fixed tube current was used without automatic tube current modulation. SAFIRE (Siemens, Munich, Germany) iterative reconstruction algorithm was used for image reconstruction on 128-detector-row CT scanner and iDose^4 (Philips Healthcare, Andover, MA) iterative reconstruction algorithm was used on 64-detector-row CT scanner. All images were reconstructed by lung filter kernel. The other scan parameters were as follows: collimation, 0.75 mm; pitch, 1.0; section thickness, 2mm.

C. Image Analysis

One radiology trainee measured CT attenuation of nodules in entire CT images.

A mean value and standard-deviation of internal attenuation were measured by circular region of interest (ROI) drawn in central area of nodules excluding periphery within 1 mm from the surface using a slice image that showed the largest dimension of the nodule. A tendency of alteration in CT attenuation of the nodules was evaluated according to the change of tube current and voltage.

Two radiology trainees blinded to the results of attenuation measurement (with 3 years of training period) evaluated the phantom images of standard-dose (120 kVp/100 mAs) and five selected low-dose (120 kVp/40 mAs, 120 kVp/20 mAs, 100 kVp/20 mAs, 80 kVp/20 mAs, 80 kVp/10 mAs) CT images obtained using 128-detector-row CT for discrimination of hyperdense nodules. These low-dose tube parameters were selected because they were thought to be representative for evaluation of low-dose and ultra-low-dose chest CT using iterative reconstruction referring to previous studies in the literature[5, 19, 20]. The threshold of 200 HU is used for the criteria of hyperdense nodule. Before the evaluation each reader had a training period with the standard dose images showing a nodule with 200 HU of mean attenuation. Each reader evaluated total 84 images of 14 nodules obtained with 6 imaging protocols using five-grade scale ; 1-Absolutely under 200 HU ; 2-Probably

under 200 HU ; 3-Equivocal attenuation ; 4-Probably over 200 HU ; 5-Absolutely over 200 HU. The accuracy of grading was analyzed comparing with actual CT attenuation of nodules. Interobserver correlation of nodule-grading between two readers was also analyzed.

D. Statistics

The mean internal attenuation and standard-deviation of ROI were evaluated by linear-regression analysis. The accuracy of nodule discrimination in five selected low-dose CT scans were compared with standard-dose CT scan by McNemar test. Interobsever correlation of nodule grading was analyzed using Cohen's kappa statistics. The Kappa strength of agreement was as follows: <0.20 poor agreement, 0.21–0.40 fair, 0.41–0.60 moderate, 0.61–0.80 good and 0.81–1.00 very good. Linear-regression analysis and Cohen's kappa statistics were performed using SPSS version 22.0 (IBM, Chicago, IL, USA)

III. RESULTS

A. CT Attenuation of Artificial Nodules

Table 1-4 shows the mean CT attenuation and standard deviation of ROI in the phantom nodules. Mean CT attenuations of 14 nodules on standard-dose using 128-detector-row CT varied from 82.4 to 316.3 HU and their standard deviations distributed from 21.2 to 118.0 HU. Mean CT attenations on standard dose using 64-detector row-CT varied from 109.4 to 402.7 HU and their standard deviations distributed from 26 to 95.8 HU. Mean CT attenuation showed an increasing tendency as the tube voltages decreased in eight nodules with mean attenuation more than 180 HU on standard-dose CT. However, nodules with lower attenuation (1, 2 and 8 on 128-detector-row CT and nodule 1 and 8 on 64-detector-row CT) showed decreasing mean CT attenuations as the tube voltage decreased. Mean CT attenuation showed negative linear relationship with tube voltage in seven nodules on 128-detector-row CT and eleven nodules on 64-detector-row CT scanners. These results were statistically significant ($p<0.05$). Tube current did not show linear relationship with mean CT attenuation on both CT scanners. Although mean attenuations of nodule 9

and 10 were below 200 HU on standard dose CT, they increased over 200 HU on low dose CTs especially with 80 kVp/10 mAs combination. Standard deviation of CT attenuation of nodules increased as the tube voltage decreased showing negative linear relationship with statistical significancy ($p<0.05$) in both scanners. In relation with the standard deviation of CT attenuation, tube current also showed statistically significant ($p<0.05$) negative linear relationship in 13 nodules on 128-detector-row CT and 9 nodules on 64-detector-row CT (Table 5 and 6). Standard deviations of nodule attenuation are considerably increased when using low voltage and low current combination (80 kVp/20 mA, or 80 kVp/15 mA) in more than 2 folds comparing with those using standard-dose in all nodules.

Table 5. Linear regression analysis of CT attenuation in 128-detector-row CT scanner

	Size	CTA on Standard-Dose (Mean ± SD)	Linear Regression of Mean CTA	Linear Regression of SD
Nodule 1	10mm	82.4 ± 32.6	HU = 45.936 + 0.210*kVp	†SD = 260.908 - 0.642*mAs - 1.565*kVp
Nodule 2	10mm	144.4 ± 26.0	HU = 132.042 + 0.145*kVp	†SD = 168.165 - 0.445*mAs - 0.906*kVp
Nodule 3	10mm	171.5 ± 27.0	HU = 191.346 - 0.195*kVp	†SD = 119.885 - 0.367*mAs - 0.519*kVp
Nodule 4	10mm	202.8 ± 27.0	†HU = 278.592 - 0.655*kVp	†SD = 150.029 - 0.399*mAs - 0.743*kVp
Nodule 5	10mm	250.5 ± 60.0	†HU = 397.848 - 1.245*kVp	†SD = 194.896 – 0.223*mAs – 1.044*kVp
Nodule 6	10mm	282.9 ± 75.8	HU = 426.545 – 1.105*kVp	†SD = 259.528 - 0.372*mAs - 1.398*kVp
Nodule 7	10mm	316.3 ± 94.3	†HU = 552.767 - 1.915*kVp	†SD = 294.122 - 0.485*mAs – 1.419*kVp
Nodule 8	7mm	98.8 ± 21.2	HU = 70.094 + 0.230*kVp	†SD = 239.557 - 0.389*mAs – 1.407*kVp
Nodule 9	7mm	148.5 ± 26.5	HU = 243.327 - 0.795*kVp	†SD = 227.009 - 0.636*mAs - 1.331*kVp
Nodule 10	7mm	169.2 ± 22.6	HU = 194.498 - 0.160*kVp	†SD = 176.885 - 0.556*mAs – 0.928*kVp
Nodule 11	7mm	216.8 ± 33.7	†HU = 306.295 - 0.735*kVp	†SD = 225.645 - 0.713*mAs - 1.209*kVp
Nodule 12	7mm	251.4 ± 65.9	†HU = 456.105 - 1.725*kVp	†SD = 203.418 - 1.040*kVp
Nodule 13	7mm	270.9 ± 118.0	†HU = 537.984 - 2.135*kVp	†SD = 367.723 - 0.420*mAs - 1.987*kVp
Nodule 14	7mm	308.1 ± 52.2	†HU = 570.575 - 2.130*kVp	†SD = 212.413 - 0.358*mAs - 1.237*kVp

CTA ; CT attenuation of nodule, SD ; standard deviation of CT attenuation

† : Statistically significant

Table 6. Linear regression analysis of CT attenuation in 64-detector-row CT scanner

	Size	CTA on Standard-Dose (Mean±SD)	Linear Regression of Mean CTA	Linear Regression of SD
Nodule 1	10mm	109.4 ± 35.8	HU = 88.373 + 0.191*kVp	†SD = 192.953 - 0.573*mAs – 0.961*kVp
Nodule 2	10mm	174.5 ± 26.9	HU = 189.521 – 0.084*kVp	†SD = 166.211 – 0.433*mAs – 0.934*kVp
Nodule 3	10mm	203.3 ± 24.1	HU = 214.827 – 0.132*kVp	†SD = 141.053 - 0.374*mAs – 0.716*kVp
Nodule 4	10mm	233.6 ± 26.0	†HU = 308.745 - 0.645*kVp	†SD = 186.312 - 0.430*mAs - 1.047*kVp
Nodule 5	10mm	307.7 ± 56.9	†HU = 486.568 – 1.566*kVp	†SD = 143.577 – 0.658*kVp
Nodule 6	10mm	320.8 ± 72.3	†HU = 556.703 – 2.031*kVp	†SD = 198.653 – 0.944*kVp
Nodule 7	10mm	402.7 ± 64.9	†HU = 688.873 – 2.420*kVp	†SD = 240.656 - 1.166*kVp
Nodule 8	7mm	123.0 ± 38.2	†HU = 93.060 - 0.346*kVp	†SD = 208.883 - 0.564*mAs - 1.056*kVp
Nodule 9	7mm	183.2 ± 32.3	†HU = 268.898 - 0.655*kVp	†SD = 214.888 - 0.541*mAs - 1.189*kVp
Nodule 10	7mm	199.2 ± 29.2	†HU = 270.746 - 0.622*kVp	†SD = 159.112 - 0.442*mAs – 0.843*kVp
Nodule 11	7mm	248.9 ± 24.1	†HU = 385.247 – 1.116*kVp	†SD = 213.558 - 0.550*mAs - 1.260*kVp
Nodule 12	7mm	288.3 ± 30.8	†HU = 466.927 – 1.536*kVp	†SD = 153.104 - 0.294*mAs – 0.801*kVp
Nodule 13	7mm	303.6 ± 95.8	†HU = 535.588 – 1.849*kVp	†SD = 282.138 - 1.499*kVp
Nodule 14	7mm	349.9 ± 53.7	†HU = 655.855 – 2.568*kVp	†SD = 190.959 - 1.090*kVp

CTA ; CT attenuation of nodule, SD ; standard deviation of CT attenuation

† : Statistically significant

B. Visual Assessment and Interobserver Correlation

Accuracies of nodule grading by visual assessment of each imaging protocol (kVp/mAs: 120/100, 120/40, 120/20, 100/20, 80/20, and 80/10) were 71.4%, 78.6%, 92.9%, 85.7%, 71.4%, 71.4% in observer 1 and 92.9%, 85.7%, 92.9%, 92.9%, 92.9%, 100% in observer 2. Mean accuracy were 78.6% and 92.8% in observer 1 and observer 2. The accuracy in five low-dose protocols were not significantly different with the accuracy in standard-dose protocol in each observer. Sensitivity and specificity of detecting hyperdense nodules more than 200 HU were not either significantly different in relation with variation of tube voltage and current. The overall accuracy between two nodule sizes were not significantly different in each observers. In the inter-observer agreement of nodule grading, moderate agreement was shown in three protocols (120 kVp/40 mAs, 120 kVp/20 mAs, 100 kVp/20 mAs) with statistical significance ($p<0.05$). Assessment in other three protocols showed poor agreement and the results were not statistically significant. (Table 7 and 8)

Table 7. Five-point grading for discrimination of hyperdense nodules in each observers

		Nodule Grading											
		120kVp/100mAs		120kVp/40mAs		120kVp/20mAs		100kVp/20mAs		80kVp/20mAs		80kVp/10mAs	
	Mean HU of nodules	Observer 1	Observer 2	Observer 1	Observer 2	Observer 1	Observer 2	Observer 1	Observer 2	Observer 1	Observer 2	Observer 1	Observer 2
Nodule 1	82.4	2	1	1	1	1	1	2	2	2	1	2	1
Nodule 2	144.4	3	1	3	2	2	2	3	2	4	2	3	2
Nodule 3	171.5	5	2	3	2	2	2	4	2	4	3	3	2
Nodule 4	202.8	5	4	4	4	3	3	4	3	4	3	4	3
Nodule 5	250.5	5	4	4	3	4	3	4	4	5	4	4	3
Nodule 6	282.9	4	4	4	4	2	4	5	3	4	4	5	4
Nodule 7	316.3	5	5	5	5	4	5	5	5	5	5	5	5
Nodule 8	98.8	2	1	1	1	1	1	1	1	1	1	1	1
Nodule 9	148.5	4	2	2	2	2	2	2	2	3	2	3	2
Nodule10	169.2	3	3	3	3	2	3	2	3	3	2	3	2
Nodule11	216.8	4	3	3	2	3	3	4	3	4	3	4	3
Nodule12	251.4	4	5	5	5	4	4	5	5	4	5	4	5
Nodule13	270.9	5	5	4	5	4	4	5	5	5	5	4	4
Nodule14	308.1	4	5	5	5	4	5	5	5	5	4	5	4

Table 8. Accuracy, sensitivity, specificity in discrimination of hyperdense nodule and inter-observer correlation of nodule grading between each readers

Tube Parameter (kVp/mAs)	Average of SD of Nodules	Reader 1					Reader 2					Kappa of Nodule Grading
		Accuracy			Sensitivity	Specificity	Accuracy			Sensitivity	Specificity	
Nodule size		7mm	10mm	Overall	Overall	Overall	7mm	10mm	Overall	Overall	Overall	
120/100	44.9 HU	71.4%	71.4%	71.4%	100%	33.3%	85.7%	100%	92.9%	100%	83.3%	0.085
120/40	53.5 HU	85.7%	71.4%	‡78.6%	100%	50%	71.4%	100%	‡85.7%	87.5%	83.3%	†0.563
120/20	65.2 HU	100%	85.7%	‡92.9%	83.3%	100%	85.7%	100%	‡92.9%	100%	83.3%	†0.545
100/20	74.9 HU	100%	71.4%	‡85.7%	100%	66.7%	85.7%	100%	‡92.9%	100%	83.3%	†0.458
80/20	106.1 HU	71.4%	71.4%	‡71.4%	100%	33.3%	100%	85.7%	‡92.9%	100%	83.3%	0.097
80/10	138.8 HU	71.4%	71.4%	‡71.4%	100%	33.3%	100%	100%	‡100%	100%	100%	0.019

† : Statistically significant ($p < 0.05$)

‡ : No statistically significant difference compared with standard-dose with the McNemar test

IV. DISCUSSION

Low-dose chest CT was introduced into lung cancer screening in 1998 in Japan, for the first time[21]. Since then, many reports have been published about the clinical implication of low-dose chest CT for screening with long debate about the worth of low-dose chest CT[22-25]. The effectiveness of the low dose-chest CT for lung cancer screening was proved in 2011 by the results of the National Lung Screening Trial (NLST), which was prospective and randomized clinical trial of high risk subjects[2]. The study concluded that screening with low-dose CT resulted in reducing the lung cancer mortality, while that with conventional chest radiograph did not. Yi et al. also reported better detection of lung cancer and higher survival rate in patients with lung cancer in non-high risk subjects of Asian population[1]. Nevertheless, it remains on the debates, such as optimal radiation dose, frequency of screening and low positive predictive value[26, 27].

Radiation exposure is one of the main problems of the CT examination. The average radiation dose of CT scan used in the NLST was 1.5mSv which equates to about 22% of the average dose of standard-dose chest CT examination[28]. Although

the carcinogenic effect related with the amount of radiation used for low-dose chest CT would be very small, it cannot be totally negligible[28, 29]. Brenner reported that a single low-dose CT scan has a fairly low risk (<0.06%) for radiation-induced lung cancer, but the risk can be increased by early screening (1.5-5% increase in high-risk group)[29]. For further reduction of radiation dose, ultralow-dose chest CT began to be used for cancer screenig, however, its clinical effectiveness is yet to be determined.

Image noise in the CT scan is mainly caused by quantum noise which significantly increases in low-dose setting of CT imaging[30]. Although the reduction of radiation dose decreases radiation-related hazard, image quality is also degraded. Poor image quality has a bad effect on the detection and characterization of lung nodule. Many reports proposed that an appropriate tube current and tube voltage should be used in the setting of low-dose chest CT screening, for maintaining adequate diagnostic imaging quality. However, proper radiation dose is still under debate. Image noise is defined as the standard deviation in a region of interest. In our study, standard deviation of CT attenuation of the nodules increased as the tube current and voltage decreased (Fig. 3). Post-processing technique of image reconstruction is one of important factors for improving image quality in low-dose

CT scan. Iterative reconstruction technique is a recently introduced technique that has become clinically applicable because increased computing power enables fast image reconstruction. Many reports have shown the benefit of iterative reconstruction for improving the image quality of low-dose chest CT[5, 11-15]. SAFIRE and iDose[4] reconstruction algorithms were used in our study.

Several features of CT examination suggest benignity of lung nodule. One of the features is the CT attenuation of lung nodule. Nodules with calcification of diffuse, central, popcorn-shaped, or laminar types are generally considered benign. CT densitometry has been investigated for determining a certain level of nodule attenuation as a threshold for benignity. Proto et al. reported that nodules with an attenuation above 200 HU can be considered as benign[16]. Siegelman et al suggested 164 HU as a threshold for discriminating benign from malignant nodules[18]. Erasmus et al. suggested that 200 HU of attenuation value is advocated by many as a good discriminator between calcified and non-calcified nodules[31].

Our study was designated to investigate for diagnostic accuracy of hyperdense nodule over 200 HU of CT attenuation in the various settings of low-dose chest CT examination. In our study, as the voltages and tube currents decreased, standard

deviation of CT attenuation increased showing negative linear correlation, representing increased image noise on low dose setting. In protocols with low voltage and low current combination (80 kVp / 20 mA, or 80 kVp / 15 mA) standard deviation of nodule attenuation increased in more than 3 folds comparing with those in standard dose protocol. These findings suggest a high degree of image noise in low voltage and low current setting, that could affect the visual assessment of nodule density. Although the mean attenuation of nodule was less affected by decreased tube voltage and current, nodules with attenuation range of 140-200 HU on standard dose setting could manifest as hyperdense nodules with a mean density above 200 HU on low voltage and low current setting especially using 80 kVp/10 mA. This finding suggests that the same attenuation criteria could not be used for hyperdense nodule on CT densitometry using low voltage and low current setting even though iterative reconstruction is used. The results of this study may be used as a guide for an adjustment of those criteria when ultralow dose CT is used for nodule densitometry.

We performed visual assessment of phantom nodules using six protocols of CT images obtained with a standard-dose and five low-dose scanning parameters. Selected low-dose setting included ultra-low-dose parameters. The mean accuracy in

discrimination of hyperdense nodule over 200HU showed 78.6% in observer 1 and 92.8% in observer 2 with mean values. A difference of accuracy between observers might represent the subjectivity in visual assessment of non-calcified hyperdense lung nodule. Two nodules (nodule 9 and 10) showed remarkable increase of mean CT attenuation over 200HU in the lowest radiation-dose setting (80kVp/10mAs). These nodules can be considered hyperdense nodules just in the lowest-dose CT scan (Fig. 4 and 5). But there was no significant difference of accuracy between standard-dose and low-dose settings in each reader. This result suggest that the low-dose chest CT including ultra-low-dose setting maintains the diagnostic accuracy in evaluating hyperdense nodule, though alteration of CT attenuation is increased. Several reports showed that subjective image quality does not reveal significant difference in low-dose chest CT using iterative reconstruction comparing with standard-dose CT using conventional FBP[32, 33]. Our result also might be affected by iterative reconstruction technique. Inter-observer agreement of nodule grading showed moderate agreement in three protocols (120 kVp/40 mAs, 120 kVp/20 mAs, 100 kVp/20 mAs) and poor aggrement in relatively lower radiation-dose groups (80 kVp/20 mAs, 80 kVp/10 mAs). Prominent image noise of lower radiation-dose CT scans is thought to make

influence in perception of nodule attenuation, but it does not significantly disturb a discrimination of hyperdense nodule when the experienced readers are adapted to the image noise of ultra-low-dose setting.

Our study has several limitations. First, there was an inherent limitation of phantom nodule. All phantom nodules used in this study were made manually and composed of mixture with polyvinyl alcohol, calcium carbonate, and 3% solution of borax. These nodules does not show a complete internal homogeneity. Internal inhomogeneity of the nodules may cause an exaggeration of CT attenuation in perception. Second, visual assessment of phantom nodules in our study was subjective method and performed by only two readers training in radiology. Discrimination of hyperdense nodule without direct measurement of ROI may require an appropriate experience. Third, we could not suggest exact radiaton dose criteria. Even though low-dose CT scans of our study showed comparable accuracy compared with standard-dose CT scan in visual assessment, actual CT attenuation of some nodules showed considerable alteration over 200 HU in low-dose setting. Finally, the number of nodules and the covered range of attenuation were relatively small and narrow. Further studies on a large scale will be necessary to ensure the

clinical application of the results of our study.

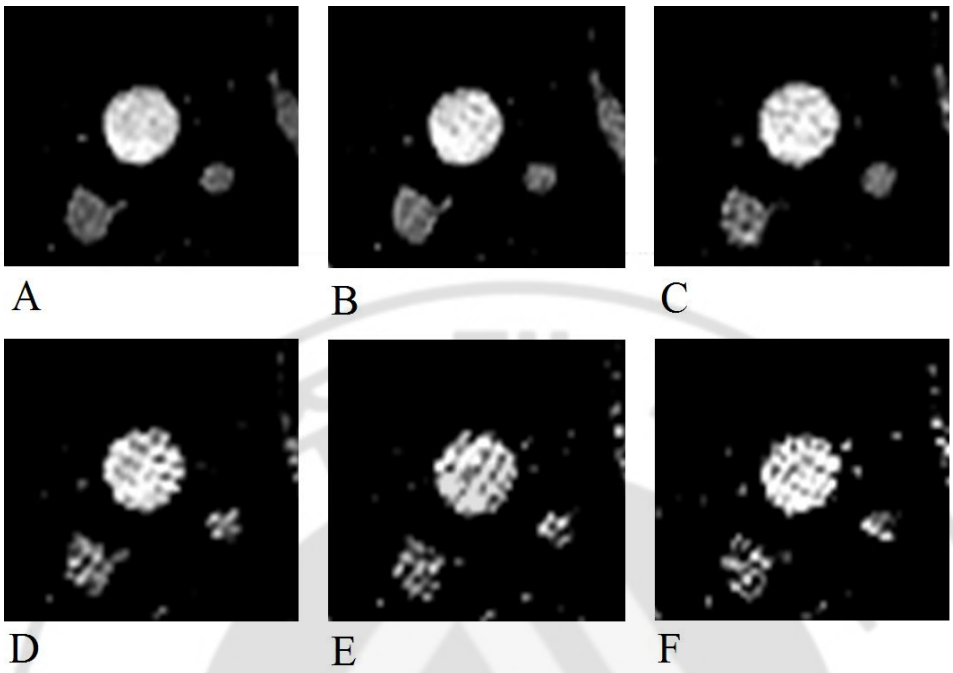

Figure 3. CT images of nodule 9 in various tube parameters obtained using 128-detector-row scanner. Note increasing image noise with low tube current. (Window width/level = 350/40)

(A)120kVp/100mAs (B)120kVp/40mAs (C)120kVp/20mAs (D) 100kVp/20mAs (E) 80kVp/20mAs (F) 80kVp/10mAs

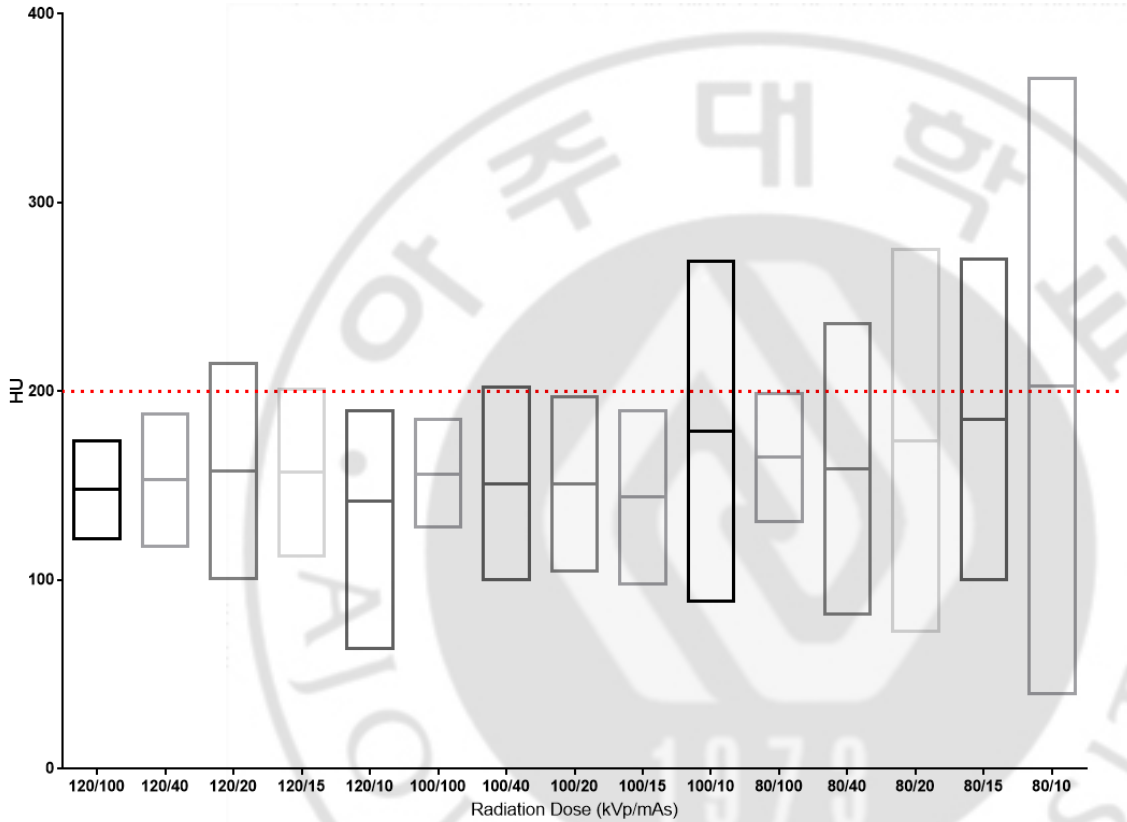

Figure 4. Floating bar diagram showing mean values (midline of the boxes) and stadard deviations (a half of height in the boxes) of the nodule 9 in 128-detector-row CT images. Note markedly increasing standard deviation of attenuation on low mAs images.

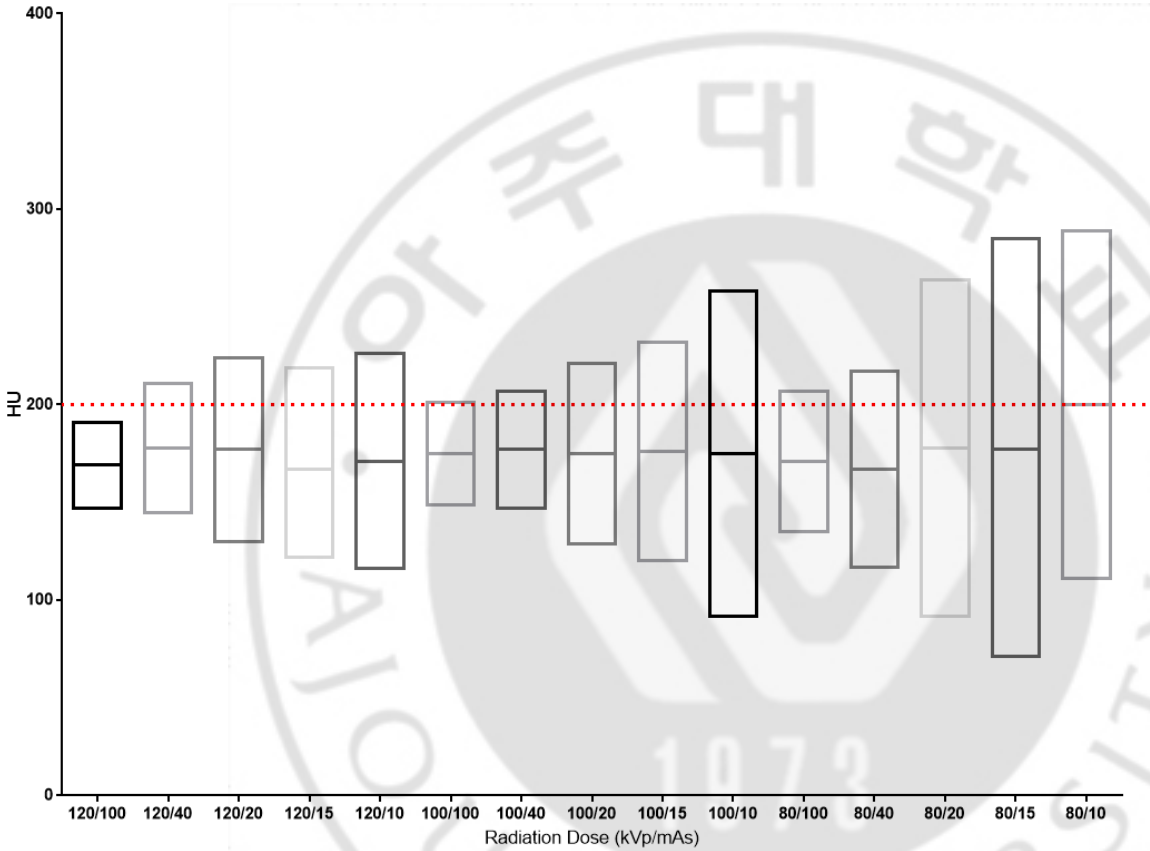

Figure 5. Floating bar diagram showing mean values (midline of the boxes) and stadard deviations (a half of height in the boxes) of the nodule 10 in 128-detector-row CT images

V. CONCLUSION

In conclusion, our study showed a high degree of attenuation change of nodules in low voltage and low current setting that suggests the need for an adjustment of attenuation criteria for determining hyperdense nodule by CT densitometry, and low-dose chest CT maintains the diagnostic accuracy in visual assessment of hyperdense lung nodule despite increased image noise.

REFERENCE

1. Yi CA, Lee KS, Shin MH, et al. Low-dose CT screening in an Asian population with diverse risk for lung cancer: A retrospective cohort study. Eur Radiol 2015;25:2335-45.
2. National Lung Screening Trial Research T, Aberle DR, Adams AM, et al. Reduced lung-cancer mortality with low-dose computed tomographic screening. N Engl J Med 2011;365:395-409.
3. Jaklitsch MT, Jacobson FL, Austin JH, et al. The American Association for Thoracic Surgery guidelines for lung cancer screening using low-dose computed tomography scans for lung cancer survivors and other high-risk groups. J Thorac Cardiovasc Surg 2012;144:33-8.
4. Saghir Z, Dirksen A, Ashraf H, et al. CT screening for lung cancer brings forward early disease. The randomised Danish Lung Cancer Screening Trial: status after five annual screening rounds with low-dose CT. Thorax 2012;67:296-301.
5. Christe A, Charimo-Torrente J, Roychoudhury K, et al. Accuracy of low-dose computed tomography (CT) for detecting and characterizing the most common CT-patterns of pulmonary disease. Eur J Radiol 2013;82:e142-50.
6. Das M, Muhlenbruch G, Heinen S, et al. Performance evaluation of a computer-aided detection algorithm for solid pulmonary nodules in low-dose and standard-dose MDCT chest examinations and its influence on radiologists. Br J Radiol 2008;81:841-7.
7. Michel JL, Reynier C, Avy G, et al. [An assessment of low-dose high resolution CT in the detection of benign asbestos-related pleural abnormalities]. J Radiol 2001;82:922-3.
8. Paul NS, Siewerdsen JH, Patsios D, et al. Investigating the low-dose limits of multidetector CT in lung nodule surveillance. Med Phys 2007;34:3587-95.
9. Yamada T, Ono S, Tsuboi M, et al. Low-dose CT of the thorax in cancer follow-up. Eur J Radiol 2004;51:169-74.
10. Zompatori M, Fasano L, Mazzoli M, et al. Spiral CT evaluation of pulmonary emphysema using a low-dose technique. Radiol Med 2002;104:13-24.
11. Willemink MJ, Leiner T, de Jong PA, et al. Iterative reconstruction techniques for computed tomography part 2: initial results in dose reduction and image quality. Eur Radiol 2013;23:1632-42.
12. Baumueller S, Winklehner A, Karlo C, et al. Low-dose CT of the lung: potential value of iterative reconstructions. Eur Radiol 2012;22:2597-606.

13. Xu Y, He W, Chen H, et al. Impact of the adaptive statistical iterative reconstruction technique on image quality in ultra-low-dose CT. Clin Radiol 2013;68:902-8.
14. Hwang HJ, Seo JB, Lee JS, et al. Radiation dose reduction of chest CT with iterative reconstruction in image space - Part I: studies on image quality using dual source CT. Korean J Radiol 2012;13:711-9.
15. Pontana F, Pagniez J, Flohr T, et al. Chest computed tomography using iterative reconstruction vs filtered back projection (Part 1): Evaluation of image noise reduction in 32 patients. Eur Radiol 2011;21:627-35.
16. Proto AV, Thomas SR. Pulmonary nodules studied by computed tomography. Radiology 1985;156:149-53.
17. Khan AN, Al-Jahdali HH, Irion KL, et al. Solitary pulmonary nodule: A diagnostic algorithm in the light of current imaging technique. Avicenna J Med 2011;1:39-51.
18. Siegelman SS, Zerhouni EA, Leo FP, et al. CT of the solitary pulmonary nodule. AJR Am J Roentgenol 1980;135:1-13.
19. Kim Y, Kim YK, Lee BE, et al. Ultra-Low-Dose CT of the Thorax Using Iterative Reconstruction: Evaluation of Image Quality and Radiation Dose Reduction. AJR Am J Roentgenol 2015;204:1197-202.
20. Kim H, Park CM, Chae HD, et al. Impact of radiation dose and iterative reconstruction on pulmonary nodule measurements at chest CT: a phantom study. Diagn Interv Radiol 2015;21:459-65.
21. Sone S, Takashima S, Li F, et al. Mass screening for lung cancer with mobile spiral computed tomography scanner. Lancet 1998;351:1242-5.
22. Bach PB. Reduced lung-cancer mortality with CT screening. N Engl J Med 2011;365:2036; author reply 2037-8.
23. Henschke CI. Re: inconsistencies in findings from the early lung cancer action project studies of lung cancer screening. J Natl Cancer Inst 2012;104:254-5; author reply 255-6.
24. Patz EF, Jr. Lung cancer screening, overdiagnosis bias, and reevaluation of the Mayo Lung Project. J Natl Cancer Inst 2006;98:724-5.
25. International Early Lung Cancer Action Program I, Henschke CI, Yankelevitz DF, et al. Survival of patients with stage I lung cancer detected on CT screening. N Engl J Med 2006;355:1763-71.

26. Ruano-Ravina A, Perez Rios M, Fernandez-Villar A. Lung cancer screening with low-dose computed tomography after the National Lung Screening Trial. The debate is still open. Arch Bronconeumol 2013;49:158-65.
27. Marshall HM, Bowman RV, Yang IA, et al. Screening for lung cancer with low-dose computed tomography: a review of current status. J Thorac Dis 2013;5 Suppl 5:S524-39.
28. Larke FJ, Kruger RL, Cagnon CH, et al. Estimated radiation dose associated with low-dose chest CT of average-size participants in the National Lung Screening Trial. AJR Am J Roentgenol 2011;197:1165-9.
29. Brenner DJ. Radiation risks potentially associated with low-dose CT screening of adult smokers for lung cancer. Radiology 2004;231:440-5.
30. Yu L, Liu X, Leng S, et al. Radiation dose reduction in computed tomography: techniques and future perspective. Imaging Med 2009;1:65-84.
31. Erasmus JJ, Connolly JE, McAdams HP, et al. Solitary pulmonary nodules: Part I. Morphologic evaluation for differentiation of benign and malignant lesions. Radiographics 2000;20:43-58.
32. Yanagawa M, Gyobu T, Leung AN, et al. Ultra-low-dose CT of the lung: effect of iterative reconstruction techniques on image quality. Acad Radiol 2014;21:695-703.
33. Vardhanabhuti V, Loader RJ, Mitchell GR, et al. Image quality assessment of standard- and low-dose chest CT using filtered back projection, adaptive statistical iterative reconstruction, and novel model-based iterative reconstruction algorithms. AJR Am J Roentgenol 2013;200:545-52.

- 국문요약 -

저선량 CT에서 다양한 촬영기법에 따른 폐결절의 석회화 발견과 음영도 변화의 팬텀 연구

아주대학교 대학원 의학과

조재용

(지도교수 : 박경주)

목적: 흉부 저선량 CT에서 다양한 선량에 따른 폐결절의 음영도 변화와 미만성 석회화의 육안적 진단정확도를 표준선량 CT와 비교하여 알아보고자 하였다.

대상 및 방법: 인공 폐결절을 삽입한 흉부 팬텀을 64-detector-row CT와 128-detector-row CT 으로 촬영하였으며 표준선량과 다양한 관전압, 관전류의 저선량을 통해 영상을 획득하였고 영상 재구성에 Iterative reconstruction 기법이 사용되었다. 인공폐결절의 평균 CT attenuation과 image noise를 표준선량과 저선량 CT영상에서 측정하였다. 표준선량과 5

개의 저선량 CT영상에서 인공폐결절의 미만성 석회화에 대하여 두명의 관찰자가 평가하여 그 진단정확도를 비교하였다.

결과: 인공폐결절의 평균 CT attenuation과 image noise는 관전압과 관전류가 감소할수록 증가하였다. 표준선량 CT영상에서 200HU 미만의 CT attenuation을 가지는 일부 폐결절들은 저선량 CT영상에서 200HU 보다 큰 CT attenuation을 보였다. 인공폐결절의 미만성 석회화에 대한 육안적 진단정확도는 표준선량 CT영상과 저선량 CT영상에서 차이를 보이지 않았다. 저선량 CT영상에 비해 표준선량 CT영상에서 관찰자간 일치도가 높았다.

결론: 저선량 CT영상에서 표준선량 CT영상에 비하여 image noise가 증가함에도 불구하고 인공폐결절의 미만성 석회화에 대한 육안적 진단 정확도가 유지됨을 확인하였다.